ACS NANO
Cite This: ACS Nano 2019, 13, 6581−6595
www.acsnano.org

ARTICLE

A Biomimetic Hierarchical Nanointerface Orchestrates Macrophage Polarization and Mesenchymal Stem Cell Recruitment To Promote Endogenous Bone Regeneration

Shan-Shan Jin,[†] Dan-Qing He,[†] Dan Luo,[‡] Yu Wang,[†] Min Yu,[†] Bo Guan,[§] Yu Fu,[∥] Zi-Xin Li,[†] Ting Zhang,[†] Yan-Heng Zhou,[†] Cun-Yu Wang,[⊥] and Yan Liu*[,†]

[†]Laboratory of Biomimetic Nanomaterials, Department of Orthodontics, Peking University School and Hospital of Stomatology, National Engineering Laboratory for Digital and Material Technology of Stomatology, Beijing Key Laboratory of Digital Stomatology, Beijing 100081, China

[‡]Institute of New Energy, China University of Petroleum (Beijing), Beijing 102249, China

[§]Beijing National Laboratory for Molecular Science, Institute of Chemistry, Chinese Academy of Sciences, Beijing 100190, China

[∥]Fourth Division, Peking University Hospital of Stomatology, Beijing 100025, China

[⊥]Laboratory of Molecular Signaling, Division of Oral Biology and Medicine, School of Dentistry, University of California Los Angeles, Los Angeles, California 90095, United States

Supporting Information

ABSTRACT: **The host immune response to bone biomaterials is vital in determining scaffold fates and bone regeneration outcomes. The nanometer-scale interface of biomaterials, which independently controls physical inputs to cells, regulates osteogenic differentiation of stem cells and local immune response. Herein, we fabricated biomimetic hierarchical intrafibrillarly mineralized collagen (HIMC) with a bone-like staggered nanointerface and investigated its immunomodulatory properties and mesenchymal stem cell (MSC) recruitment during endogenous bone regeneration. The acquired HIMC potently induced neo-bone formation by promoting $CD68^+CD163^+$ M2 macrophage polarization and $CD146^+STRO\text{-}1^+$ host MSC recruitment in critical-sized bone defects. Mechanistically, HIMC facilitated M2 macrophage polarization and interleukin (IL)-4 secretion to promote MSC osteogenic differentiation. An anti-IL4 neutralizing antibody significantly reduced M2 macrophage-mediated osteogenic differentiation of MSCs. Moreover, HIMC-loaded-IL-4 implantation into critical-sized mandible defects dramatically enhanced bone regeneration and $CD68^+CD163^+$ M2 macrophage polarization. The depletion of monocyte/macrophages by clodronate liposomes significantly impaired bone regeneration by HIMC, but did not affect MSC recruitment. Thus, in emulating natural design, the hierarchical nanointerface possesses the capacity to recruit host MSCs and promote endogenous bone regeneration by immunomodulation of macrophage polarization through IL-4.**

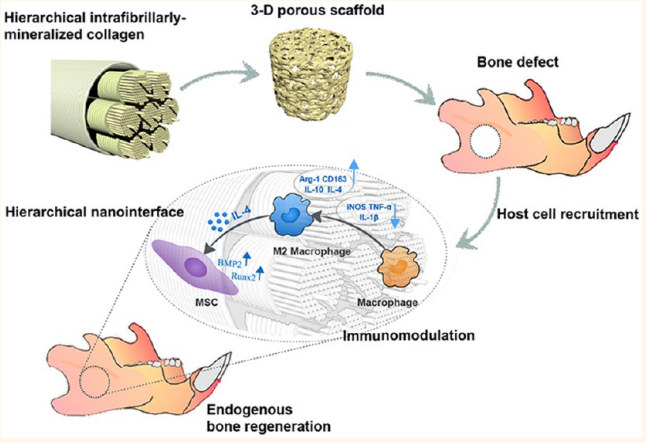

KEYWORDS: *biomimetic nanointerface, osteoimmunomodulation, macrophage, mesenchymal stem cells, interleukin-4, endogenous bone regeneration*

Biomaterials have been developed in response to an inadequate supply of organs and tissues in massive bone defects secondary to traumatic, congenital, and post-oncologic deformities.[1,2] Successful biomaterial-mediated bone regeneration depends on complex biomaterial−host interactions involving the immune response and stem cell recruitment and differentiation.[3] After biomaterial implantation, the host reactions initiate with innate immune system activation. The

Received: January 18, 2019
Accepted: May 24, 2019
Published: May 24, 2019

DOI: 10.1021/acsnano.9b00489
ACS Nano 2019, 13, 6581−6595

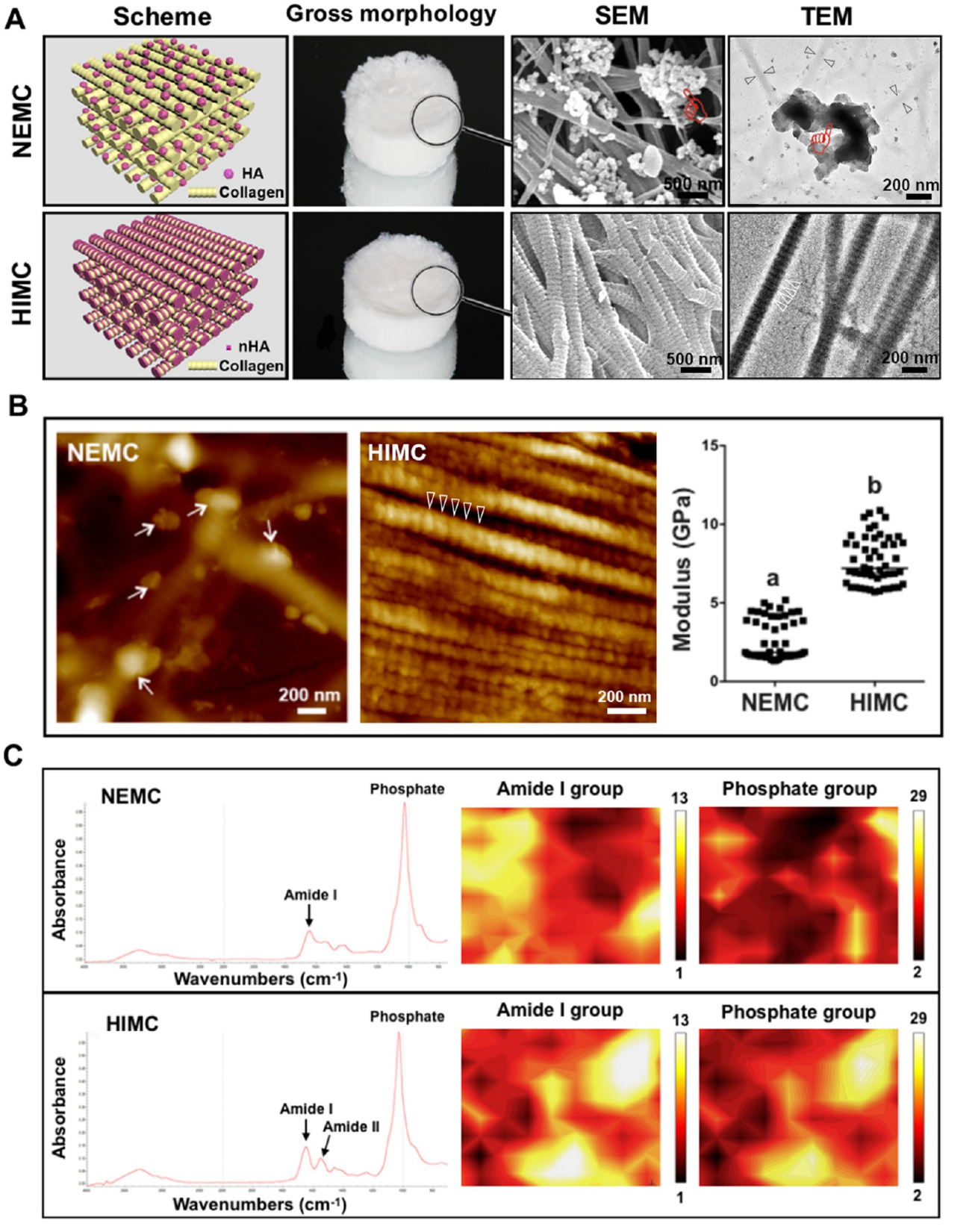

Figure 1. Physiochemical properties of mineralized collagen. (A) Scheme, gross morphology, and nanostructure of scaffolds. HIMC showed a bone-like staggered nanotopography with distinct *D-periods* (white open arrowheads). Pointers: HA clusters. Black open arrowheads: Unmineralized collagen. (B) Young's modulus of NEMC and HIMC by AFM. Arrows: HA; white open arrowheads: *D-periods*. The different lowercase letters indicate a significant difference between the two groups. (C) Micro-FTIR spectra and mappings of NEMC and HIMC. The color scale indicates the spectral intensity.

DOI: 10.1021/acsnano.9b00489
ACS Nano 2019, 13, 6581−6595

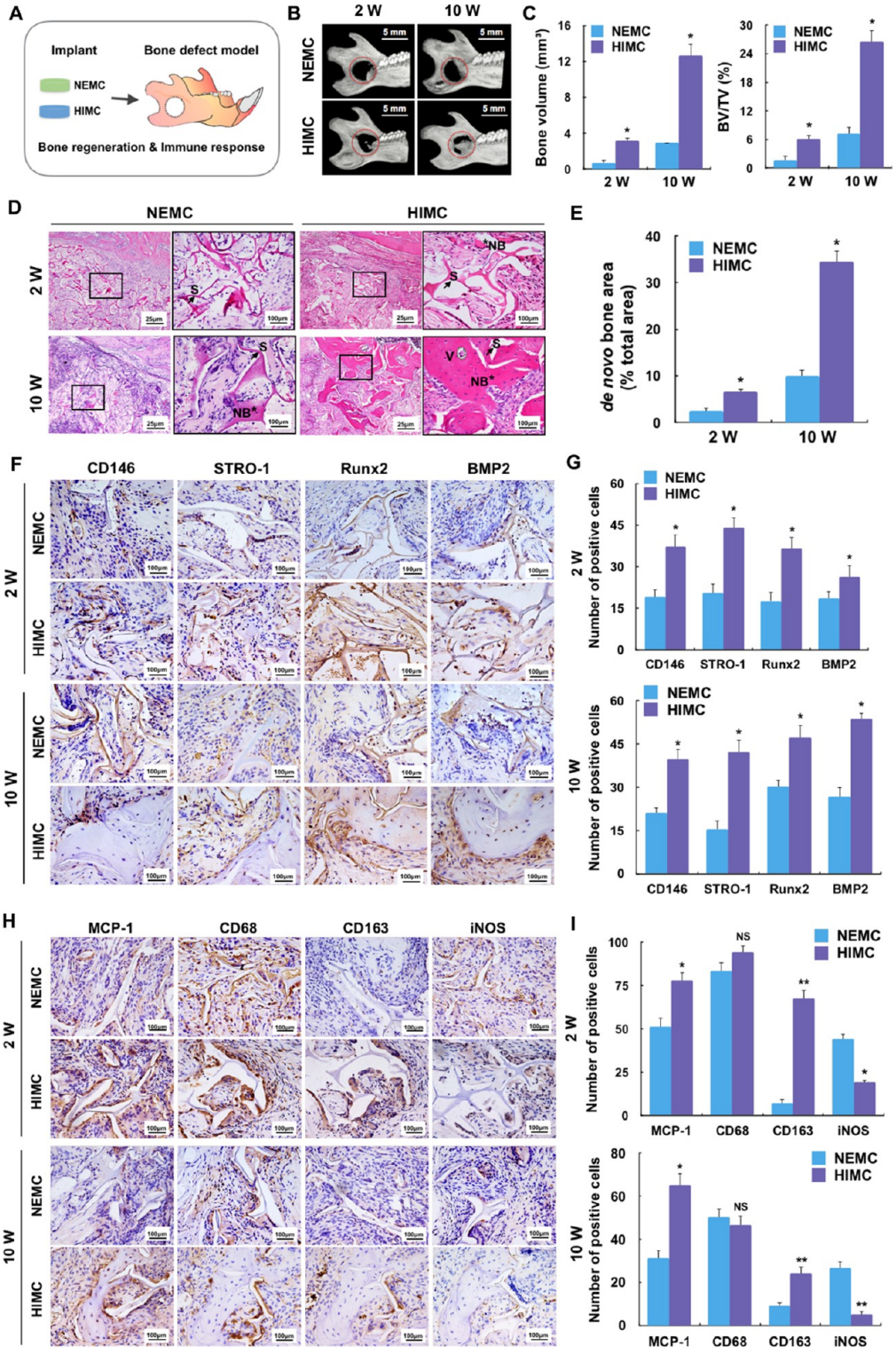

Figure 2. Endogenous bone regeneration by HIMC. (A) Schematic diagram of a bone defect and implantation. (B) Representative micro-CT images of NEMC and HIMC post-implantation for 2 and 10 weeks. (C) BV and BV/TV analyses at 2 and 10 weeks. (D) H&E staining of the engineered bone in rat mandibles at 2 weeks and 10 weeks. NB: Neo-bone (asterisks); S: scaffold (arrows); V: vessel (green circles). (E) Semiquantification of *de novo* bone area in (D). (F) Representative immunohistochemistry staining of CD146, STRO-1, Runx2, and BMP2 in defect areas. The HIMC group showed more $CD146^+STRO\text{-}1^+$cells and increased expression levels of Runx2 and BMP2 in the defect area at 2 and 10 weeks. (G) Semiquantification of positively stained cells in (F). (H) Representative immunohistochemical images of macrophage polarization in defect areas. At each time point, an increased expression level of MCP-1 and an enhanced number of $CD68^+CD163^+$ M2 macrophages were observed in the HIMC group, whereas $CD68^+iNOS^+$ M1 macrophages were dominant in the NEMC group. (I) Semiquantification of positively stained cells in (H). *: $P < 0.05$ *versus* NEMC, **: $P < 0.01$ *versus* NEMC, and NS: not significant.

DOI: 10.1021/acsnano.9b00489
ACS Nano 2019, 13, 6581−6595

innate immune cell subsets are certified as key players in biomaterial remodeling and a potential target for immune-mediated bone regeneration.[4−6]

Among various innate immune cells, macrophages are one of the most vital effectors in biomaterial-related immune reactions. After *in vivo* implantation of biomaterials, macrophages are the earliest cells recruited to the implant area. Also, the long-term immune reactions to biomaterials are primarily determined by macrophages.[7] Adapting to variable microenvironments, macrophages tactically shift to the classically activated M1 phenotype, or alternatively, the M2 phenotype, to mediate inflammation and maintain tissue homeostasis, respectively.[8,9] M1 macrophages intensify inflammation by producing cytokines such as inducible nitric oxide synthase (iNOS) and tumor necrosis factor (TNF)-α, whereas M2 macrophages facilitate tissue healing by producing anti-inflammatory cytokines such as arginase-1 (Arg-1) and interleukin (IL)-10.[10] It has been reported that the shift to a different macrophage polarization may influence the outcomes of tissue regeneration after scaffold implantation.[11] A switch to M2 macrophage polarization is judged to be a favorable adaptation.[12] Furthermore, macrophages are essential for effective mineralization of osteoblasts and *in vivo* bone formation by secreting osteoinductive factors, such as transforming growth factor β and bone morphogenetic protein 2 (BMP2).[13,14] Given the importance of macrophages in material-related immune response and bone formation, the response of macrophages to biomaterial scaffolds has been widely studied, in an attempt to resolve their osteoimmunomodulatory properties.[15]

The role of biomaterial scaffolds, such as bone grafts, has shifted from a biologically passive structural role to one in which material properties, such as the surface topography and chemistry, orchestrate bone regeneration by regulating stem cells and the local microenvironment. This strategy relies on the development of a target-specific biomaterial scaffolding system that can mimic natural bone hierarchy and surface nanotopography, to offer an appropriate microenvironment for recruitment and differentiation of host cells. Surface nanotopography of biomaterials, which potently manipulates physical inputs to host cells, modulates osteogenic stem cell differentiation and the local immune response, thereby determining bone regenerative outcomes.[16] Recently, we successfully fabricated hierarchical intrafibrillarly mineralized collagen (HIMC) by mimicking the surface chemistry and hierarchical nanotopography of natural bone, using a biomimetic bottom-up mineralization approach.[17−22] This biomimetic hierarchical nanointerface determines the mechanical properties of the mineralized collagen[19] and fate of stem cells[20] and regenerates neo-bone with a similar micro- and nanostructure to that of natural bone.[21,22] While the bone-like nanointerface has potent osteoinductive properties, the underlying molecular mechanisms that promote bone formation are not fully understood. This study was aimed to investigate the mechanisms of endogenous bone regeneration, with a focus on how the bone-like nanointerface affects the local microenvironment. To this end, we examined macrophage polarization induced by the biomimetic hierarchical nanointerface and its association with native osteo-related MSC recruitment.

RESULTS AND DISCUSSION

Biomimetic Hierarchical Nanointerface Assembly and Characterization. The extracellular matrix (ECM) of native bone consists mainly of collagen fibrils with nanohydroxyapatites (nHAs) embedded in collagenous gap zones, resulting in hierarchical intrafibrillar mineralization with a staggered pattern.[23] As such, mimicking the natural ECM is considered as a promising strategy for developing ideal bone substitutes to orchestrate the bone regeneration process, by regulating the local microenvironment and promoting cellular interactions with the ECM. Herein, emulating natural design, HIMC was produced using a modified bottom-up approach with two steps involving poly(acrylic acid)-calcium (PAA-Ca) precursor preparation and hierarchical nanostructure assembly. The self-assembly of tropocollagen molecules into fibrils and the hierarchical arrangement of PAA-Ca in collagenous gap regions occur simultaneously. In scanning electron microscopy (SEM) and transmission electron microscopy (TEM) images, HIMC showed a bone-like staggered nanotopography with nHAs deposited mainly in the collagenous gap regions, leading to obvious *D-periodic* banding patterns. The absence of PAA in the mineralization solution resulted in hydroxyapatite (HA) cluster formation, arranged randomly around the collagen fibrils; in turn, this created extrafibrillarly mineralized collagen without a bone-like hierarchical nanostructure (NEMC) (Figure 1A).[17−19,21] This finding was further confirmed by atomic force microscopy (AFM) results. The parallel-aligned HIMC fibrils showed distinct *D-periodic* banding patterns and a higher Young's modulus from 5.76 to 10.89 GPa, whereas NEMC fibrils were distributed irregularly with a lower modulus from 1.31 to 5.184 GPa (Figure 1B). It has been shown that appropriate pore size and swelling ratio of a three-dimensional (3-D) scaffold play important roles in cell attachment and growth, and tissue formation.[24] Under the same lyophilizing condition, the acquired 3-D HIMC and NEMC showed a similar porosity with interconnected pores of 154.2 ± 19.6 μm (Figure S1). However, the water absorption capability of HIMC (26.43 ± 3.93%) was much higher than that of NEMC (13.89 ± 2.49%), which was probably due to the fact that HA clusters on the collagen surface in NEMC prohibited water absorption. Furthermore, HIMC exhibited a better resistance toward cyclic loads mimicking physiological conditions (Figure S2), whereas NEMC collapsed when an uniaxial compression loads on.[21]

The chemical components and spatial mineral/matrix distribution in mineralized collagen at the micron level were measured by using a micro-Fourier transform infrared spectroscopy (FTIR) (Figure 1C). Both HIMC and NEMC displayed typical collagen (1577−1727 cm^{-1}) and phosphate (900−1200 cm^{-1}) peaks, an indication of similar chemical constituents. The FTIR mappings showed a coincident spatial distribution of the amide I and phosphate groups in HIMC, demonstrating that the minerals deposited inside the collagen fibrils. In contrast, the two chemical groups were distributed differently in NEMC, which might indicate that the minerals were outside the fibrils without a close chemical correlation to collagen. These findings are consistent with SEM and TEM results. Furthermore, the higher mineral/matrix ratio of HIMC indicated a higher level of mineralization, which contributes to a higher Young's modulus for HIMC.

Increasing MSC Recruitment in Endogenous Bone Regeneration by HIMC. To understand how the bone-like hierarchy affects the local microenvironment and contributes to endogenous bone regeneration, HIMC and NEMC scaffolds, without xenogenous stem cells or cytokines loading, were implanted into rat mandible defects (Figure 2A). Two weeks after HIMC implantation, obvious neo-bone formation was detected in the defect area, and at 10 weeks post-implantation,

DOI: 10.1021/acsnano.9b00489
ACS Nano 2019, 13, 6581−6595

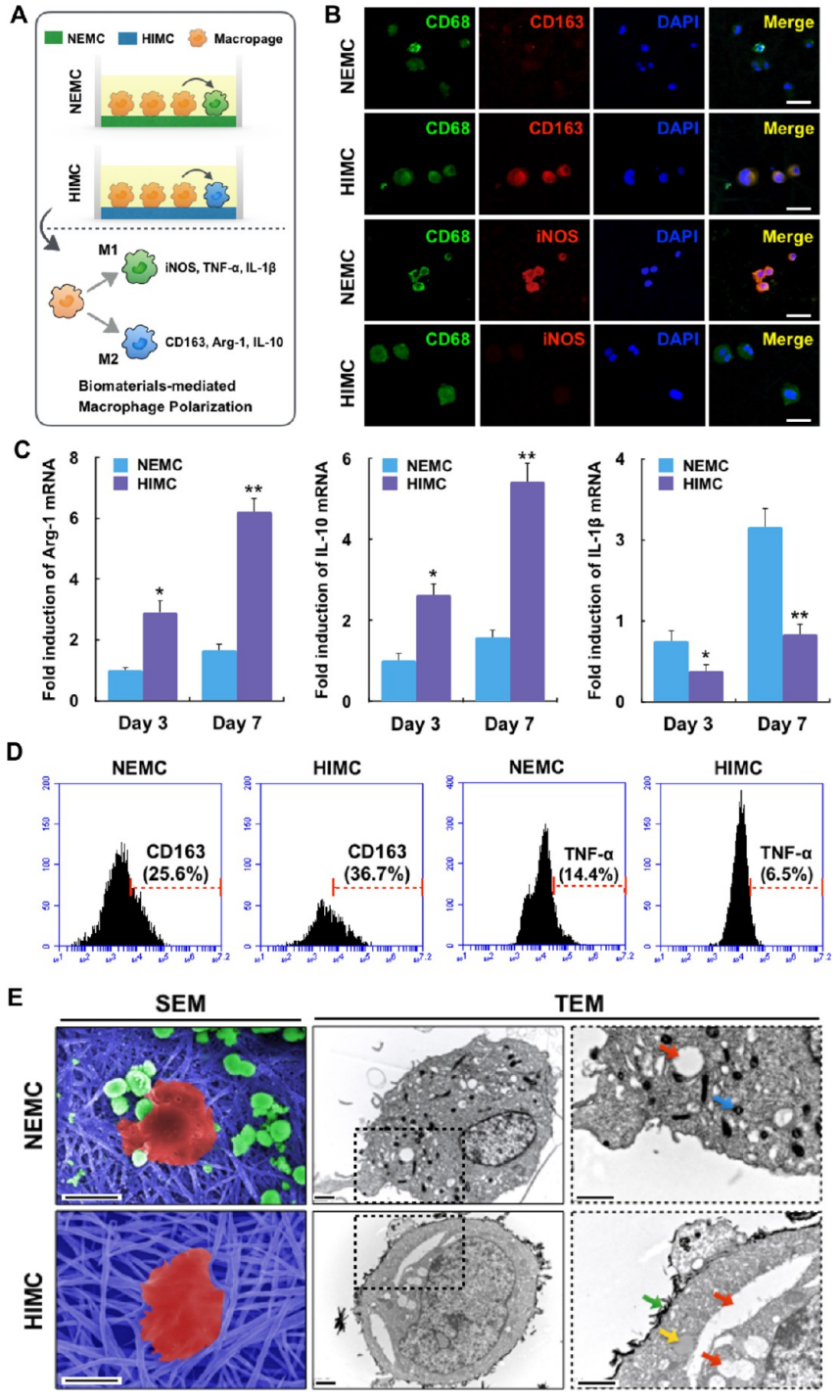

Figure 3. Macrophage polarization *in vitro*. (A) Schematic diagram of biomaterial-mediated macrophage polarization. (B) Immunofluorescent staining of macrophages with CD68 (green), CD163 or iNOS (red), and nuclei (blue) after 3 days seeded on NEMC and HIMC. The HIMC group showed more CD 68$^+$CD163$^+$ M2 macrophages, whereas CD 68$^+$iNOS$^+$ M1 macrophages were detected in the NEMC group. Scale bar = 5 μm. (C) Relative mRNA expressions of macrophage polarization-related genes at 3 and 7 days. M2 macrophage polarization-related anti-inflammatory genes (IL-10, Arg-1) were significantly upregulated in the HIMC group at each time point. However, the M1 macrophage-related pro-inflammatory gene (IL-1β) expression level was much lower in the HIMC group. *: $P < 0.05$ *versus* NEMC, **: $P < 0.01$ *versus* NEMC. (D) Flow cytometry showing an enhanced expression of the M2 macrophage marker CD163 and a decreased expression of the M1 macrophage marker TNF-α in the HIMC + THP-1 group on day 3. (E) Morphology and nanostructure of macrophages seeded on NEMC and HIMC by SEM and TEM. Red arrows: Vacuoles; yellow arrow: lysosome; blue arrow: primary lysosome; and green arrow: undegraded scaffolds. Scale bar = 10 μm for SEM and 1 μm for TEM.

the neo-bone volume (BV) was increased dramatically. On the contrary, limited neo-bone was regenerated in the defect margin in the NEMC group at both 2 and 10 weeks (Figure 2B). In the control group without implants, the defect area showed only a slight change at the 2 and 10 week time points, indicating a reliable animal defect model (Figure S3). Quantitative data showed that the BV and ratio of BV to tissue volume (BV/TV) in the HIMC group were significantly higher than those in the

DOI: 10.1021/acsnano.9b00489
ACS Nano 2019, 13, 6581−6595

NEMC group at both time points (Figure 2 C). Consistent with the radiographic results, hematoxylin and eosin (H &E) staining revealed a large amount of fibrous bone with blood vessels in the defect center of the HIMC group, whereas little neo-bone formed in the defect margin in the NEMC and control groups (Figure 2D,E).

Homing host stem cells to defect areas is a key factor for successful bone regeneration. When bone tissue sustains pathological injury, MSCs are the main stem cells mobilized from the bone marrow and recruited to the lesion site, and then differentiate into osteoblasts for bone repair.[25,26] It has been shown that osteoinductive biomaterials could adsorb endogenous growth factors from blood circulation, which could in turn promote MSC recruitment to regenerate new bone.[27] Here, immunohistochemistry staining demonstrated that the recruited cells expressed both CD146 and STRO-1 (the surface markers for MSCs) in the defect area at 2 weeks and lasted for 10 weeks (Figure 2F,G). The number of $CD146^+STRO\text{-}1^+$ cells in the HIMC group was significantly higher than that in the NEMC group at both time points. Meanwhile, a large number of runt-related transcription factor 2- (Runx2-, the principal osteogenic transcription factor) and BMP2- (an inducer of osteogenic differentiation) positive cells were observed in the defect area at 2 weeks and increased obviously at 10 weeks in the HIMC group. Taken together, HIMC, compared with NEMC, is capable of recruiting more MSCs to promote osteogenesis in the defect area, which is similar to our previous findings.[28]

Promoting M2 Macrophage Polarization in Endogenous Bone Regeneration by HIMC. Growing evidence suggests that the local microenvironment may influence host-cell behavior and the pathological disease process. Uncontrolled inflammation status, such as persistent macrophage activation, plays a pivotal role in the pathogenesis of chronic inflammatory diseases, which may also influence the immune-regulated osteogenesis process and induce the development of bone metabolism-related diseases such as osteoarthritis.[29,30] Whether the biomaterial scaffolds are capable of modulating the host immune response to provide an appropriate microenvironment for osteogenesis becomes vital in determining the quality and efficiency of endogenous bone regeneration. Macrophages, a major constituent of the innate immune system, act as a critical role in the material-induced immune response; additionally, their flexibility allows them to shift to different phenotypes under specific microenvironments.[29,31] After implantation of HIMC as a bone graft, monocyte chemoattractant protein-1 (MCP-1) expression was enhanced at 2 weeks and lasted to 10 weeks, indicating immune cell recruitment to the defect area of HIMC during the bone regeneration process (Figure 2H,I). Moreover, large numbers of $CD68^+$ (94.5 ± 3.7) and $CD163^+$ M2 macrophages (67.6 ± 4.7) were observed in the HIMC group at 2 weeks, whereas the number of $iNOS^+$ M1 macrophages was very low (19.3 ± 1.1). Interestingly, while the number of positively stained macrophages decreased at 10 weeks, $CD163^+$ M2 macrophages remained dominant in the HIMC group. On the contrary, $iNOS^+$ M1 macrophages (44.3 ± 2.6) were the main positively stained cells and remained activated from 2 to 10 weeks in the NEMC group. In the control group without implants, no positive staining of M1 (*i.e.*, iNOS) or M2 (*i.e.*, CD163) macrophage-related markers but some positive staining of pan-macrophage marker CD68 was identified in the defect area at either time point (Figure S4). This result indicates that macrophage polarization happens when macrophages interact with scaffolds and there are almost no polarized macrophages upon arrival. Previous research has demonstrated the involvement of M1/M2 macrophage phenotypes in the early inflammatory response and late wound healing process.[32] A M1/M2 ratio variation can modulate the severity of several chronic diseases.[30,33,34] Consistent with previous studies, our data demonstrate that HIMC implantation into the defect area provokes M2 macrophage polarization, which may help to alleviate inflammation status and contribute to the bone regeneration process.

HIMC Inducing M2 Macrophage Polarization *in Vitro*. To further explore whether and how HIMC induces M2 macrophage polarization, we seeded human THP-1 monocytes on HIMC and NEMC and analyzed the phenotypes of THP-1-derived macrophages (Figure 3A). CD163, Arg-1, and IL-10 were defined as M2 macrophage markers, and iNOS, IL-1β and TNF-α were used as M1 macrophage markers. Using these markers, immunofluorescent staining, real time-polymerase chain reaction (PCR), and flow cytometry were applied to characterize macrophage polarization induced by the two mineralized collagen types. Immunofluorescent staining showed that after 3 days of culture, $CD68^+CD163^+$ M2 macrophages were observed on HIMC, whereas the macrophages on NEMC expressed M1 macrophage markers CD68 and iNOS (Figure 3B). Real-time PCR analysis revealed that the HIMC group macrophages expressed much higher levels of the M2-macrophage-related genes Arg-1 and IL-10 and lower levels of M1-macrophage-related gene IL-1β on days 3 and 7, compared to the NEMC group (Figure 3C). To further confirm the phenotypes of differentiated macrophages, we performed flow cytometry analysis, which showed an upregulated expression level of the M2-macrophage marker CD163, of 36.7%, in the HIMC group compared to 25.6% in the NEMC group, but a down-regulated expression level of the M1-macrophage marker TNF-α, of 6.5%, in the HIMC group compared to 14.4% in the NEMC group (Figure 3D). In summary, these results indicate that HIMC steers macrophage polarization toward the M2 phenotype.

Physical cues in the ECM microenvironment may directly regulate M1/M2 macrophage polarization. To understand how the biomimetic hierarchical nanointerface regulates macrophage polarization, SEM and TEM were applied to compare the morphology and ultrastructure of macrophages between NEMC and HIMC (Figure 3E). SEM showed that macrophages seeded on NEMC commonly adhered to the HA clusters; however, in the HIMC group, the macrophages were spread along the collagen fibrils. It has been reported that HA steers the polarization of macrophages to the M1 direction,[35] whereas the degradation of collagen is closely linked to the M2 phenotype.[36] Nanoparticles are normally taken up through endosomal or lysosomal vesicles; the intracellular location and translocation of nanoparticles are directly related to the function and status of the cells.[37] TEM images showed numerous lysosomes in the NEMC group; a few electron-dense particles appeared to be isolated, without vacuole encapsulation within the cytoplasm. In contrast, pieces of material were observed outside the membrane of macrophages seeded on HIMC; several vacuoles and lysosomes appeared to be fused to one another, indicating an apparent larger vacuole formation after vesicle fusion. The acidic lysosome has a degradative capacity due to its internal abundant hydrolases enclosed by the organelle membrane. When the membrane is impaired, the lysosome would release lots of hydrolases and exogenous materials, which might in turn harm the neighboring organells.[38] Thus, we

DOI: 10.1021/acsnano.9b00489
ACS Nano 2019, 13, 6581−6595

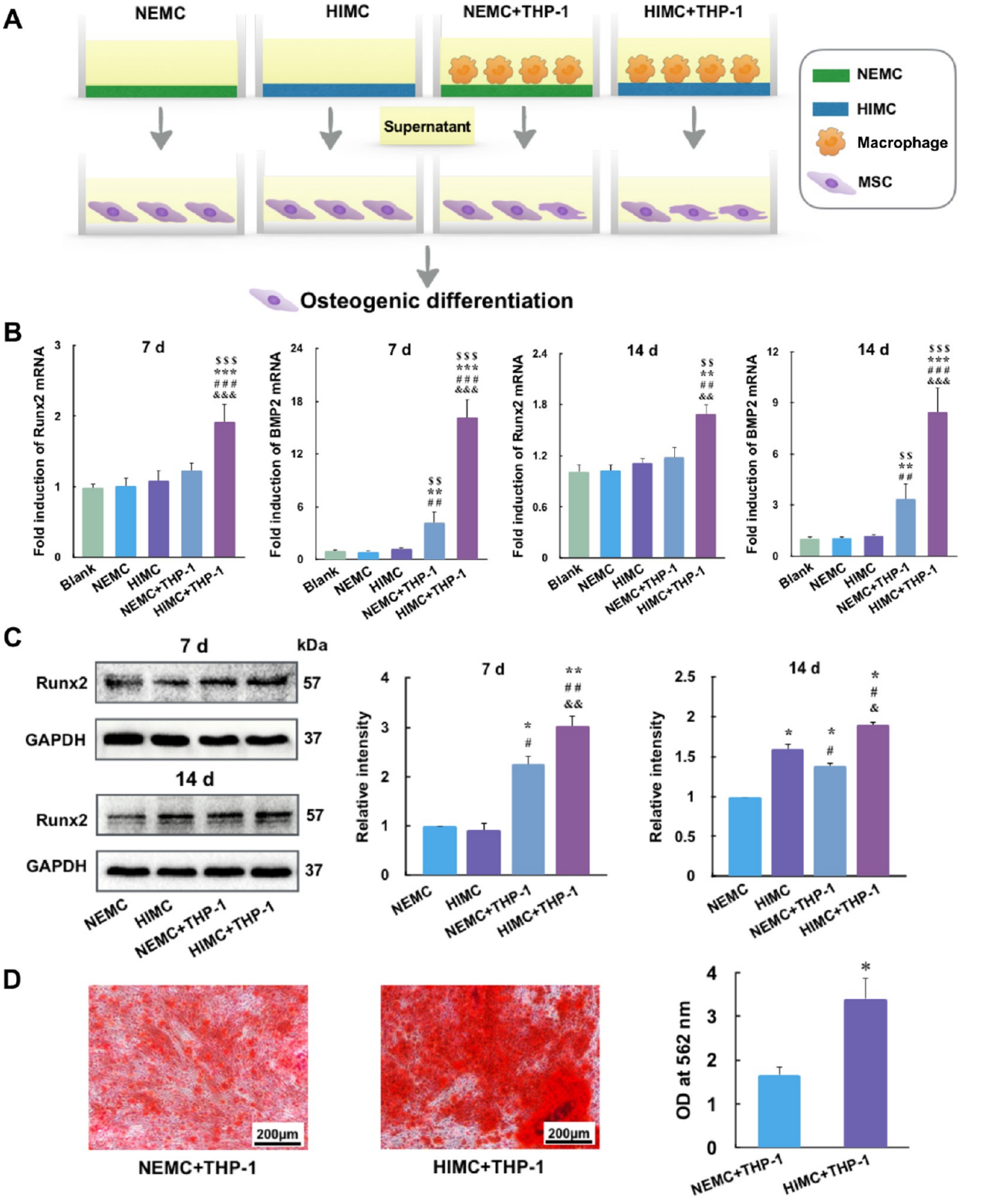

Figure 4. Association between macrophage polarization and MSC osteogenesis. (A) Schematic illustration. (B) Relative mRNA expressions of Runx2 and BMP2 in MSCs stimulated by different conditioned media for 7 and 14 days. Blank: MSCs cultured with unconditioned medium. $$: $P < 0.01$, $$$: $P < 0.001$ *versus* blank; **: $P < 0.01$, ***: $P < 0.001$ *versus* NEMC; ##: $P < 0.01$, ###: $P < 0.001$ *versus* HIMC; &&: $P < 0.01$, &&&: $P < 0.001$ *versus* NEMC+THP-1. (C) Western blot results of Runx2 expressions in MSCs on days 7 and 14. *: $P < 0.05$, **: $P < 0.01$ *versus* NEMC; #: $P < 0.05$, ##: $P < 0.01$ *versus* HIMC; &: $P < 0.05$, &&: $P < 0.01$ *versus* NEMC + THP-1. (D) ARS staining of MSCs on day 21 and semiquantification of mineralized nodules. *: $P < 0.05$.

deduced that the electron-dense materials in the NEMC-group macrophages may be the undegraded HA released by the damaged lysosome, which may be associated with the further release of inflammatory cytokines. On the contrary, several vacuoles and lysosomes appeared to fuse in macrophages seeded on the HIMC, indicating a strong capacity to turn over

DOI: 10.1021/acsnano.9b00489
ACS Nano 2019, 13, 6581−6595

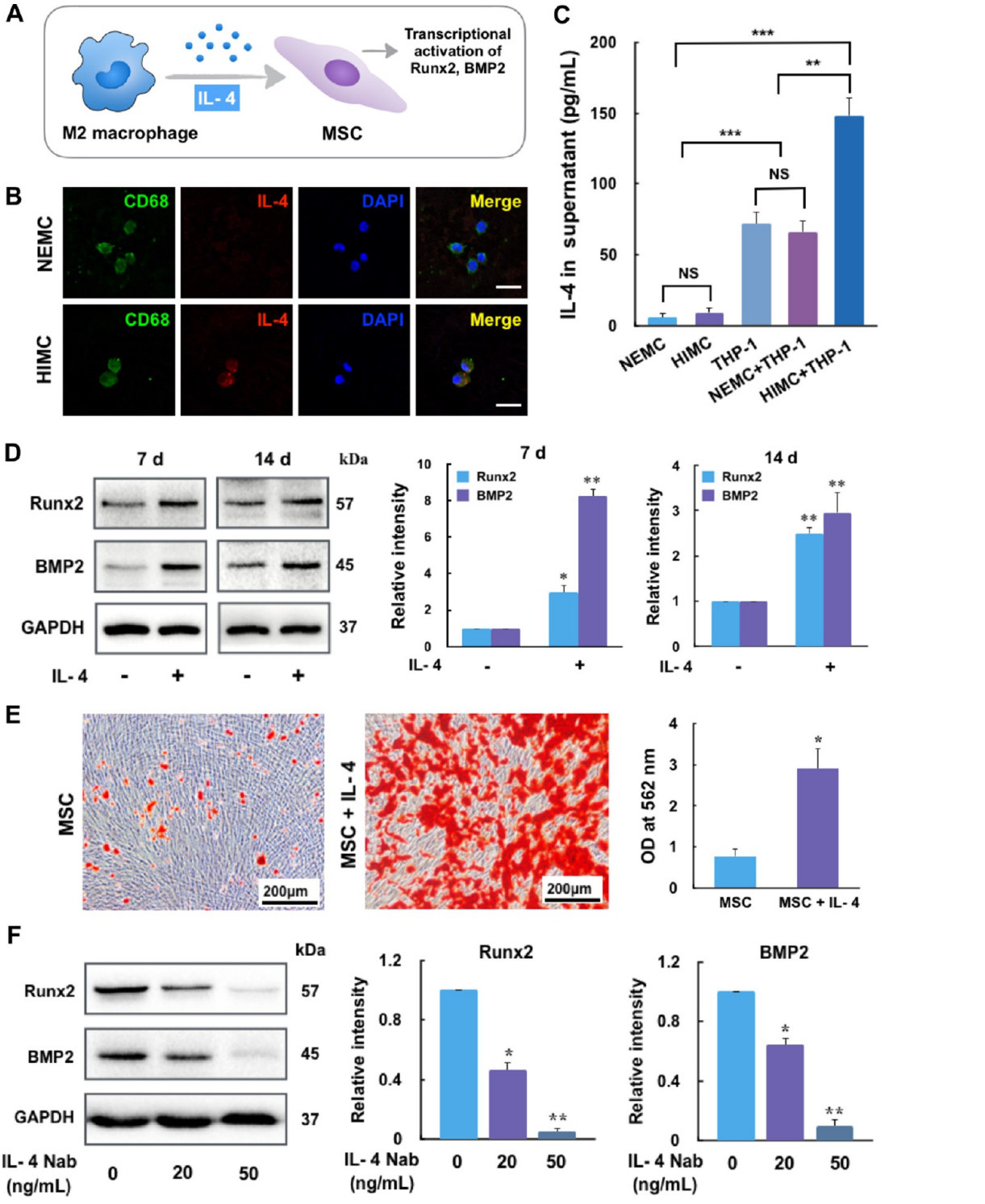

Figure 5. Osteogenic differentiation of MSCs by IL-4 stimulation. (A) Schematic illustration. (B) Immunofluorescent staining of CD68 (green), IL-4 (red), and nuclei (blue) after macrophages seeded on the NEMC or HIMC for 3 days. Scale bar = 5 μm. (C) Secretion of macrophage-associated cytokine IL-4 at 7 days. (D) Western blot results of Runx2 and BMP2 expressions in MSCs stimulated by IL-4 for 7 and 14 days. (E) ARS staining of MSCs with or without IL-4 and semiquantification of mineralized nodules. (F) Western blot results of Runx2 and BMP2 expressions in MSCs treated by an IL-4 neutralizing antibody (Nab) for 7 days. *: $P < 0.05$, **: $P < 0.01$, ***: $P < 0.001$, NS: not significant.

mineralized collagen by an intracellular pathway. Furthermore, the degraded HIMC readily excluded from the cell by exocytosis. Micron-size particles of HA also elicit a significant dose-dependent pro-inflammatory macrophage response. These results suggest that the micron-size HA clusters (4.39 ± 0.54 μm) of NEMC may be the origin of the M1 polarization induction, whereas M2 macrophages represent the principal cell type in charge of collagen turnover of HIMC, with a similar hierarchical nanointerface to that of natural bone. Our findings support a notion that M2 macrophage polarization significantly strengthens the ability of ECM turnover in an intracellular pathway.[36] It would be intriguing to investigate whether HIMC-

DOI: 10.1021/acsnano.9b00489
ACS Nano 2019, 13, 6581−6595

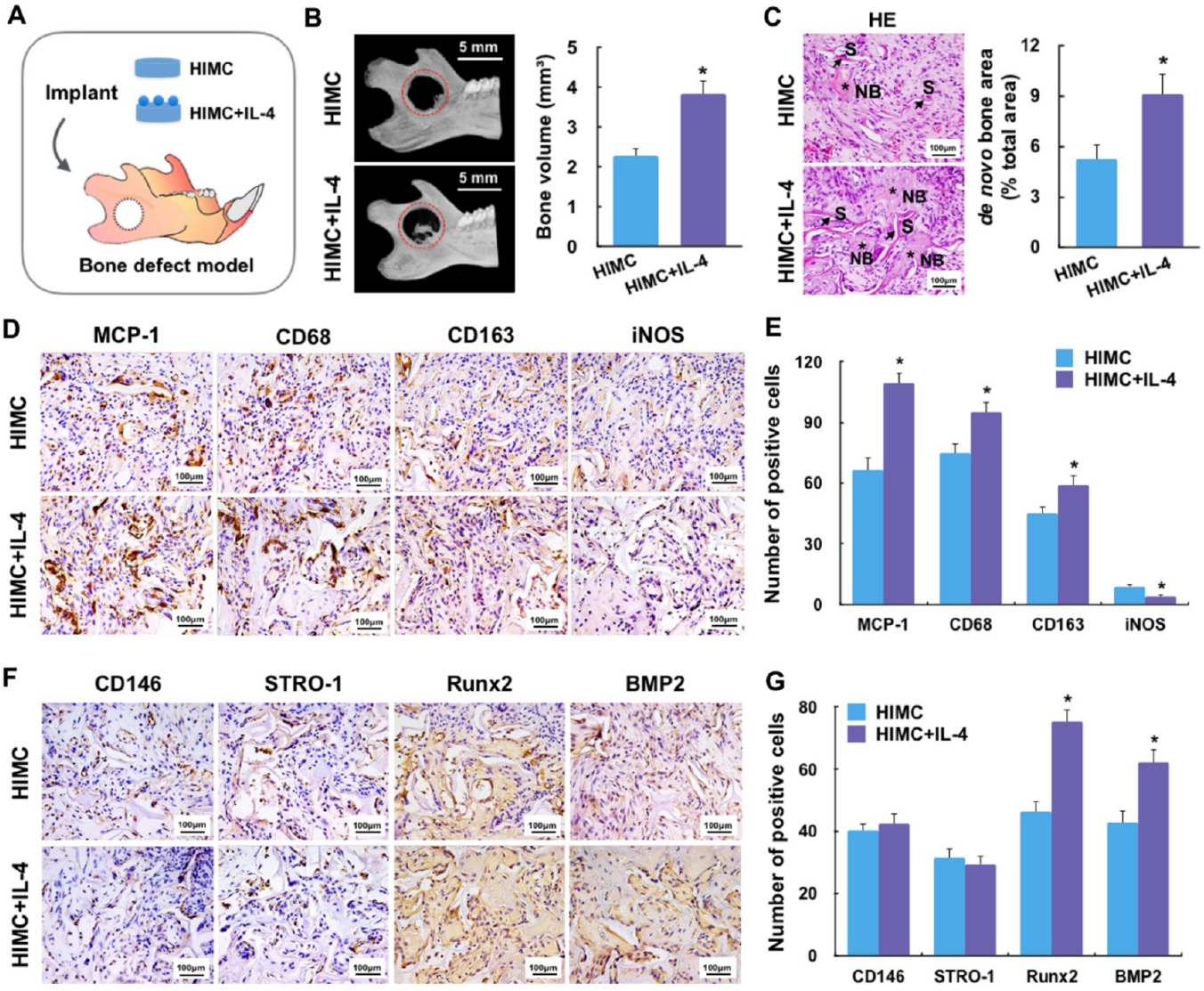

Figure 6. Endogenous bone regeneration by HIMC loaded with IL-4. (A) Schematic illustration. (B) Representative micro-CT images of HIMC and HIMC loaded with IL-4 post-implantation for 2 weeks and the BV and BV/TV of different groups. (C) H&E staining of the engineered bone at 2 weeks. S: scaffold (arrows); NB: new bone (asterisks). A semiquantitative analysis showed IL-4 promoted neo-bone formation on the HIMC scaffold. (D) Representative immunohistochemical images of macrophage polarization in defect areas. At 2 weeks, an increased expression of MCP-1 and enhanced numbers of $CD68^+CD163^+$ M2 macrophages were observed in the HIMC + IL-4 group compared with the HIMC group. (E) Semiquantification of positively stained cells in (D). (F) Representative immunohistochemistry staining of CD146, STRO-1, Runx2, and BMP2 in defect areas. (G) Semiquantification of positively stained cells in (F). There were no statistical differences in $CD146^+$ or $STRO\text{-}1^+$ between the two groups, whereas the HIMC + IL-4 group showed enhanced expressions of Runx2 and BMP2 at 2 weeks. *: $P < 0.05$ *versus* HIMC.

mediated-M2-polarized macrophages exert dual effects on material degradation and ECM synthesis in future.

Promoting MSC Differentiation by M2-Polarized Macrophages. To further investigate how the bone-like hierarchical nanointerface promotes endogenous neo-bone formation and whether it is influenced by macrophage polarization, THP-1 cells were seeded onto NEMC (NEMC + THP-1) and HIMC (HIMC + THP-1) for 7 days, and the supernatants were collected and added to cultured human bone marrow MSCs to determine their effects on MSC osteogenic differentiation. The supernatants from the scaffolds only (NEMC, HIMC) were also added to cultured MSCs as controls (Figure 4A). The MSCs cultured with the conditioned medium from the HIMC + THP-1 group exhibited a highly branched, elongated morphology. Cells in the NEMC and HIMC groups were spindle-shaped with few branching points (Figure S5). The highly branched morphology appears to be an intracellular signal that simulates osteogenic differentiation of MSCs.[39] This was confirmed by mRNA expression and the protein levels of Runx2 and BMP2.

After incubation with the supernatant from the HIMC + THP-1 group without osteogenic induction, the MSCs expressed the highest levels of Runx2 at days 7 and 14, whereas no marked change in Runx2 was detected in the MSCs cultured with the conditioned media from the other groups at both time points. Similar results were found in the BMP2 gene expression levels of the HIMC + THP-1 group. Compared to the NEMC and HIMC groups, the BMP2 gene expression in the NEMC + THP-1 group was slightly higher, but still much lower than that of the HIMC + THP-1 group at both time points (Figure 4B). A

DOI: 10.1021/acsnano.9b00489
ACS Nano 2019, 13, 6581−6595

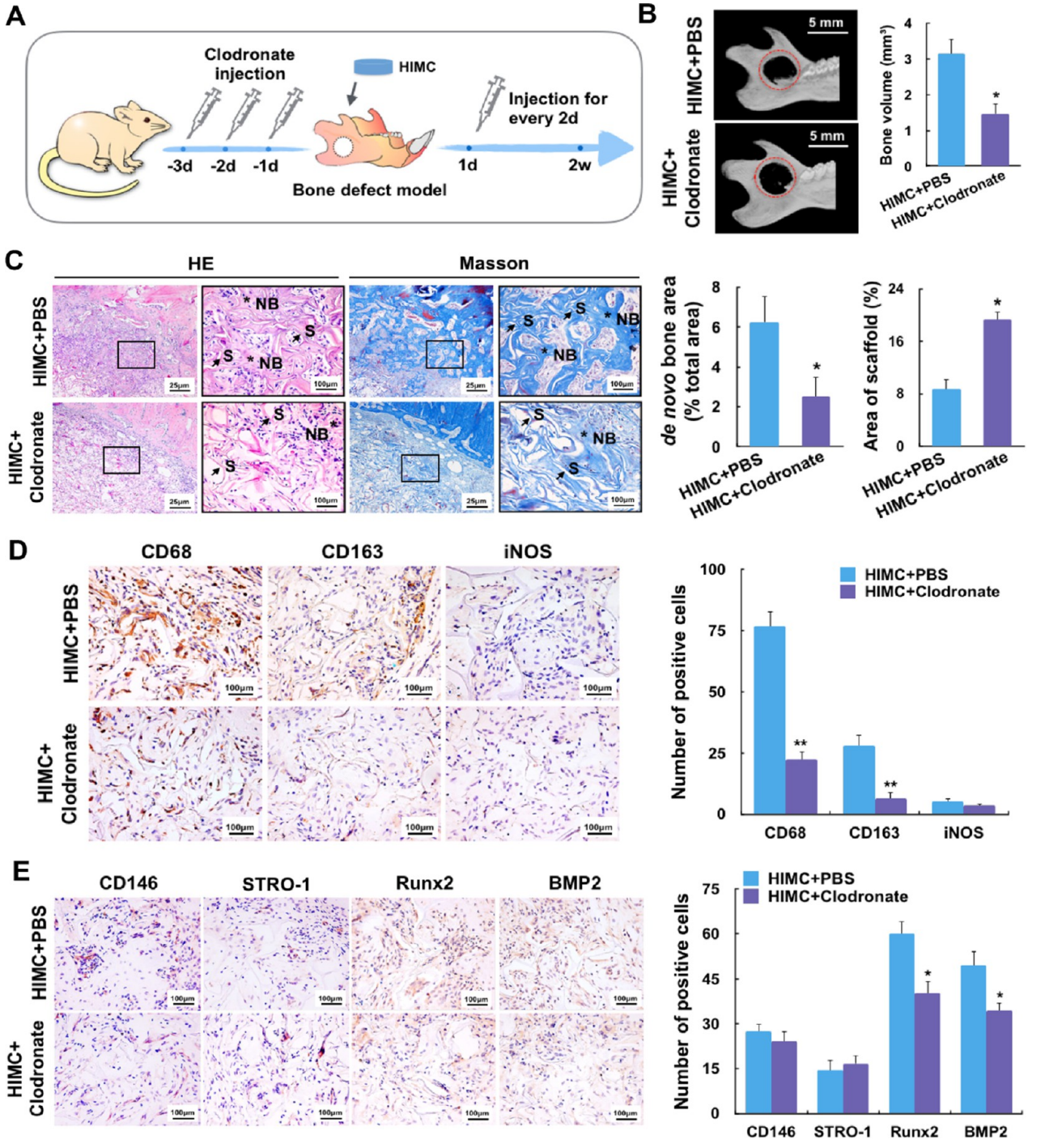

Figure 7. Monocyte/macrophage depletion impairs bone regeneration by HIMC. (A) Schematic illustration. (B) Representative micro-CT images of HIMC post-transplantation in rat mandible defects at 2 weeks and the BV of different groups. (C) H&E and Masson stainings of the engineered bone in rat mandibles at 2 weeks. S: scaffold (arrows); NB: new bone (asterisks). Semiquantitative analyses revealed clodronate injection impaired neo-bone formation and scaffold degradation of HIMC. (D) Representative immunohistochemical images of macrophage polarization in defect areas. $CD68^+$ macrophages dramatically reduced in the HIMC + Clodronate group and the expression of M2 macrophage marker CD163 were significantly downregulated as well. (E) Representative immunohistochemistry staining of CD146, STRO-1, Runx2, and BMP2 in defect areas. Semiquantification of positively stained cells showed that there were no statistical differences in $CD146^+$ or $STRO\text{-}1^+$ between the two groups, whereas the HIMC + Clodronate group exhibited decreased expression levels of Runx2 and BMP2 at 2 weeks. *: $P < 0.05$, **: $P < 0.01$.

similar trend was found in the protein expressions. Western blot revealed that the Runx2 expression in the HIMC + THP-1 group was significantly enhanced compared with that in the other three groups at both time points (Figure 4C). These findings are consistent with the results of previous similar studies, specifically that biomaterials could facilitate macrophage polarization to M2 phenotype, which in turn promotes MSC osteogenesis by upregulation of BMP2 expression.[40] In addition, alizarin red S (ARS) showed that the size and quantity of the mineral nodules generated by MSCs in the HIMC + THP-1 group were much

DOI: 10.1021/acsnano.9b00489
ACS Nano 2019, 13, 6581−6595

larger than the NEMC + THP-1 group (Figure 4D). Taken together, both the *in vivo* and *in vitro* findings demonstrate that M2 macrophage polarization induced by HIMC interacts with MSCs to promote osteogenic differentiation and mineralization of MSCs for new bone regeneration.

MSC Osteogenesis and Bone Regeneration by IL-4 Stimulation. To investigate how biomimetic hierarchical nanointerface-mediated M2-polarized macrophages promote MSC osteogenesis, IL-4, one of the most important cytokines secreted by M2 macrophages, was tested by immunofluorescence and enzyme-linked immunosorbent assay (ELISA) (Figure 5A). Immunofluorescence staining revealed that the macrophage marker CD68 co-expressed with IL-4 in the HIMC group, whereas few IL-4$^+$ cells were shown in the NEMC group (Figure 5B). ELISA results demonstrated that more than 2-fold of IL-4 was expressed in the supernatants in the HIMC + THP-1 group (148.43 ± 12.88 pg/mL) compared with the NEMC + THP-1 (67.16 ± 7.87 pg/mL) and THP-1 (72.66 ± 8.09 pg/mL) groups. Little IL-4 could be detected in both the HIMC and NEMC groups (Figure 5C). To explore whether IL-4 contributes to MSC osteogenesis, we then added IL-4 to the cultured MSCs, and the protein levels of bone-related genes and the mineralization potential of the MSCs were tested. Western blot showed that Runx2 and BMP2 expressions in MSCs increased significantly after IL-4 incubation for 7 and 14 days (Figure 5D). After incubation for 21 days, the mineralization potential of MSCs was enhanced, for increased calcium deposition and mineralized nodule formation, as shown by ARS (Figure 5E). To further confirm the positive contribution of IL-4 to MSC osteogenesis, we used an anti-human IL-4 neutralizing antibody to inhibit the IL-4 activities in the supernatants. Western blot demonstrated that the elevated expressions of Runx2 and BMP2 in the supernatants from the HIMC + THP-1 group were blocked by the IL-4 neutralizing antibody (Figure 5F). IL-10, another important anti-inflammatory cytokine secreted by M2 macrophages, was also examined. Although HIMC could also promote IL-10 secretion in macrophages, no obvious positive effect of IL-10 on MSC osteogenesis was observed (Figure S6). Thus, the enhancement of MSC osteogenesis was mainly due to increased IL-4 secretion, which is an activator of M2 macrophage polarization and can also be secreted by activated M2 macrophages to mediate anti-inflammatory and regulatory processes.[41] Similarly, a previous study showed that IL-4 is capable of converting polarized M1 into an M2 phenotype, which would enhance osteogenesis of preosteoblastic MC3T3 cells by co-culture.[42]

To examine how IL-4 exerts biological effects *in vivo*, an HIMC scaffold loaded with IL-4 (HIMC + IL-4) was implanted into critical-sized defects in rat mandibles (Figure 6A). After implantation for 2 weeks, more neo-bone was regenerated in the defect area in the HIMC + IL-4 group. Quantitative data revealed that the BV and BV/TV of the defect area were dramatically enhanced in the HIMC + IL-4 group compared to the HIMC group at 2 weeks (Figure 6B). H&E staining showed that IL-4 promoted neo-bone formation on the HIMC scaffold, evident by the semiquantitative analysis (Figure 6C). Furthermore, M1/M2 macrophage infiltration was also detected by immunohistochemistry at 2 weeks (Figure 6D). In the HIMC + IL-4 group, with increased expression of MCP-1 (109.3 ± 5.5), more CD68$^+$ macrophages (95.2 ± 5.1) infiltrated the defect area. The number of CD163$^+$ M2 macrophages (59.1 ± 4.6) increased dramatically in the HIMC + IL-4 group, whereas the number of iNOS$^+$ M1 macrophages (4.2 ± 0.9) decreased (Figure 6E). Meanwhile, immunohistochemistry results showed an increase in the number of Runx2-positive (75.1 ± 4.1) and BMP2-positive (62.3 ± 4.2) cells in the defect area at 2 weeks in the HIMC + IL-4 group. However, the numbers of CD146$^+$ and STRO-1$^+$ cells were similar between the two groups, indicating that IL-4 might not facilitate MSC recruitment (Figure 6F,G). This finding was further confirmed by a transwell migration assay (Figure S7). Consistent with *in vitro* studies, our data demonstrated that IL-4 further enhances bone regeneration in HIMC implantation, by promoting M2 macrophage polarization and MSC osteogenic differentiation.

Impairing Bone Formation by Monocyte/Macrophage Depletion. To deeply confirm the vital function of the host immune reactions to biomaterials in bone regeneration outcomes, we depleted monocyte/macrophages by injection of clodronate liposomes in rats.[43] After implantation of HIMC in rat mandible defects for 2 weeks (Figure 7A), the neo-bone volume decreased by more than 2-fold in the group treated with clodronate liposomes (HIMC + Clodronate) compared with the group treated with phosphate buffered saline (PBS, HIMC + PBS) (Figure 7B,C). Similarly, a previous study showed that the ectopic bone formation stimulated by tricalcium phosphate was blocked by monocyte/macrophage depletion.[44] Interestingly, from H&E and Masson stainings, more remnant scaffold was observed in the HIMC + Clodronate group, due to clodronate liposome inhibition of osteoclastogenesis.[44] The osteoclasts degraded the mineralized collagen in the manner which involves internalization into intracellular vesicles, providing space for osteoblasts to get in and constructing neo-bone matrix.[45] From immunohistochemical staining, CD68$^+$ macrophages in the HIMC + Clodronate group (22.5 ± 3.1) dramatically reduced about 71% of the HIMC + PBS group (76.8 ± 5.9), verifying the validity of monocyte/macrophage depletion. The expression of M2 macrophage marker CD163 was significantly downregulated as well in the HIMC + Clodronate group, while there was no difference in the iNOS$^+$ M1 macrophage number between the HIMC + Clodronate group and HIMC + PBS group (Figure 7D). Furthermore, the numbers of CD146$^+$ and STRO-1$^+$ cells were similar between the two groups, confirming that macrophage did not influence MSC recruitment. However, macrophage depletion greatly impaired MSC osteogenesis, evident by the expression levels of Runx2 and BMP2 (Figure 7E). Taken together, the lack of macrophages stemming from the host immune response would impair biomaterial-mediated bone regeneration.

It should be noted that the local immune response after biomaterial implantation may not be restricted to macrophage activation. A previous study has showed that silicified collagen scaffolds induce bone regeneration and angiogenesis *via* monocyte immunomodulation.[46] The present work demonstrates that the biomimetic hierarchical nanointerface encourages host M2 macrophage polarization and promotes MSC recruitment and osteogenic differentiation, thus providing insight into biomaterial-guided endogenous bone regeneration. Future research will focus on other immune cells, such as neutrophils, in the innate response and T cells in the adaptive response and their contributions to hierarchical nanointerface-guided neo-bone regeneration.

CONCLUSIONS

The molecular mechanisms by which a bone-like hierarchical nanointerface promotes bone regeneration and repair were elucidated in the present study. We showed that HIMC has a

DOI: 10.1021/acsnano.9b00489
ACS Nano 2019, 13, 6581−6595

Scheme 1. Potential Molecular Mechanism of How M2 Macrophage Polarization Activated by a Biomimetic Hierarchical Nanointerface Contributes to Endogenous Bone Regeneration

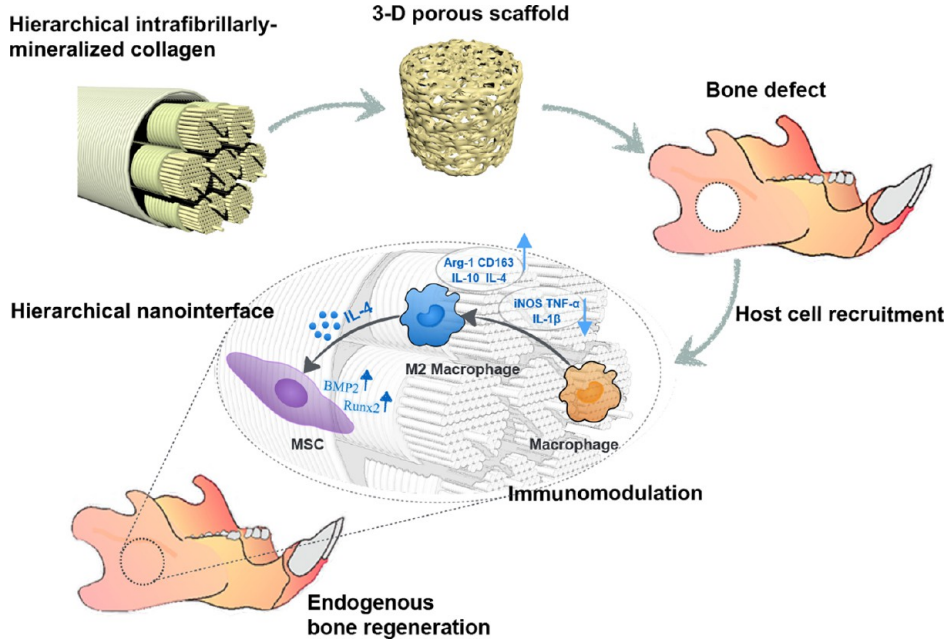

dual role in endogenous bone regeneration, by promoting both MSC recruitment and M2 macrophage polarization, which subsequently enhances MSC osteogenic differentiation and ultimately enhances bone formation (Scheme 1). The macrophages were spread along the collagen fibril of HIMC, with the fusing vacuoles and lysosomes, indicating a strong capacity of M2 macrophage to turn over HIMC by an intracellular pathway. On the contrary, macrophages adhered to the micron-size HA clusters of NEMC, which might trigger an inflammatory response of macrophages. We further revealed that HIMC intrinsically promotes M2 macrophage polarization with IL-4 secretion, which strongly enhances MSC osteogenesis and bone regeneration. These enhancing effects could be blocked by monocyte/macrophage depletion. Taken together, M2 macrophage polarization provoked by the biomimetic hierarchical nanointerface makes important contributions to endogenous bone regeneration, and IL-4, a key cytokine of M2 macrophage polarization, has a critical role during this process. These findings could give important inspiration for developing biomimetic materials for tissue regeneration in an osteoimmunomodulation perspective.

METHODS

Preparation and Characterization of Scaffolds. HIMC was achieved through a modified, biomimetic bottom-up method.[21] In brief, tropocollagen solution (Corning) was continually dropped into a dialysis flask (3500 Da) in the rate of 1 mL/min for 7 days. The flask was soaked in a mineralization solution containing 136.9 mM NaCl, 2.7 mM KCl, 8.3 mM Na_2HPO_4, 1.25 mM $K_2HPO_4{\cdot}3H_2O$, 0.25 mM poly(acrylic acid) , 3.08 mM Na_3N, and 0.2 g/mL of white Portland cement (Lehigh Cement Co.). Without poly(acrylic acid) in the solution, NEMC formed. The mineralization process was performed for 7 days at room temperature in a moisture chamber to reduce volatilization. To prepare 3-D scaffolds, the fibrillized collagen was collected by centrifugation and stirred until formation of a just-castable suspension. Then, the suspension was poured into the cavities of 48-well polystyrene culture plates, frozen for 24 h at −30 °C, and lyophilized to create 3-D sponge-like scaffolds with a similar porosity for the animal experiment.

SEM (Hitachi S-4800) and TEM (JEOL JEM-1011) were applied to observe the micro and nanotopography of scaffolds. For TEM examination, mineralized collagen was embedded in epoxy resin, sectioned with an ultramicrotome (Leica), and collected on copper grids. For water absorption test, 3-D scaffolds were weighted at dry condition (W_{dry}) and after soaked in PBS for 24 h (W_{wet}). The swelling ratio (SR, %) of the 3-D scaffolds was calculated using the equation below:

$$\mathrm{SR}\ (\%) = (W_{wet} - W_{dry})/W_{dry} \times 100$$

Micro-Fourier Transform Infrared Spectroscopy. To test the chemical components and spatial mineral/matrix distribution in different scaffolds, a LUMOS stand-alone FTIR (Bruker, USA) was used as before.[21] Briefly, mineralized collagen was collected on MirrIR slides and scanned at a resolution of 1 cm^{-1}. Spectra were acquired with an aperture size of 100 μm × 100 μm. The absorbance peaks at 1577−1727 cm^{-1} (collagen) and 900−1200 cm^{-1} (mineral) were plotted as color-coded maps to achieve the spatial mineral/matrix distribution.

Atomic Force Microscopy. The nanostructure and nanomechanics of mineralized collagen were analyzed by AFM (Dimension Icon, Bruker, USA) using a relative comparison method under ambient conditions (room temperature).[21] The samples were assembled onto freshly cleaved mica, and three scans were performed in each sample. The obtained property maps with 512 × 512 pixels were analyzed using a NanoScope 14.12 software. For every map, five regions of interest were randomly chosen, and the median value represented the value in that region of interest.

Animal Models. Critical-sized defects[47] with 5 mm diameter were prepared in adult Sprague−Dawley rat mandibles to assess the bone regeneration potential of mineralized collagen. The procedures were authorized by the Animal Use and Care Committee of Peking University (LA2014218). The 3-D HIMC ($N = 6$) and NEMC ($N = 6$) scaffolds were sterilized by ethylene oxide, immersed in α-MEM (Gibco, USA) containing 1% penicillin/streptomycin overnight at 4 °C, and implanted into defects in the absence of seed cells and cytokines. The control group ($N = 6$) was without any implants. All of the rats were sacrificed after implantation for 2 or 10 weeks, and the mandibles were removed and fixed in 10% formalin.

For bone regeneration of HIMC with IL-4, the sterilized HIMC scaffolds ($N = 6$) were immersed in α-MEM containing 1% penicillin and IL-4 (500 ng/mL, Pepro Tech) overnight at 4 °C and implanted

DOI: 10.1021/acsnano.9b00489
ACS Nano 2019, 13, 6581−6595

into defects. All of the rats were sacrificed after implantation for 2 weeks, and the mandibles were fixed in 10% formalin.

For bone regeneration of HIMC in the absence of macrophages, rats were separated into two groups: one group (HIMC + Clodronate) was intraperitoneally injected with clodronate liposomes (50 mg/kg, Netherlands) to deplete monocytes/macrophages; the other group (HIMC + PBS) received liposome-encapsulated PBS. All of the rats received injections every day prior to 3 days of HIMC implantation. After implantation, injections were performed every 2 days until all the rats were sacrificed at 2 weeks.

Micro-CT Analysis. To analyze neo-bone formation, the fixed mandibles were scanned by a Skyscan 1174 micro-CT system (Bruker, Belgium) at a resolution of 20 μm. The acquired axial images were imported into a NRecon and CTvox software for 3-D reconstruction. BV and BV/TV calculations were performed by a CTAn software (gray value >1000).

H&E, Masson, and Immunohistochemical Stainings. After micro-CT scanning, the samples were decalcified in 10% ethylenediaminetetraacetic acid for 4 weeks, dehydrated in ethanol, and embedded in paraffin. Consecutive 4 μm-thick horizontal sections were obtained from the defect area and then stained with H&E and Masson's trichrome for new bone and remnant scaffold assessment.

Immunohistochemistry was carried out using a two-step detection kit (Zhongshan Golden Bridge Biotechnology, China) as before.[28] Briefly, specimens were immersed in antigen retrieval solution for 20 min, blocked for 30 min with 5% bovine serum albumin (BSA), and subsequently incubated with primary antibodies against rat CD146 (Abcam) and Stro-1 (eBioscience) for stem cell surface markers, Runx2 and BMP2 (Abcam) for osteogenesis markers, monocyte chemoattractant protein-1 (MCP-1, Abcam) for a mononuclear phagocyte recruitment marker, CD68 (Serotec) for a pan-macrophage marker, CD163 (Santa Cruz) for a M2 marker, and iNOS (Abcam) for a M1 marker at 1:100 dilution overnight at 4 °C. After rinsing thoroughly in PBS, the horseradish peroxidase-conjugated secondary antibodies (Zhongshan Golden Bridge Biotechnology) were dropped onto slides. Each group is composed of more than three slides, and each slide was observed using a Zeiss light microscopy at the defect area including the scaffolds ($N > 3$).

Macrophage Response to HIMC *in Vitro*. *Cell Culture.* Human THP-1 monocytes were induced to differentiate into macrophages by phorbol myristate acetate treatment for 24 h at 37 °C. The 6-well plates or coverslips of 25 mm diameter with HIMC (HIMC) or NEMC (NEMC) films were sterilized using 75% ethanol for 2 h and then under ultraviolet light for 2 h before use. After THP-1 derived macrophage adherence, cells were cultured for 3 and 7 days for detection of macrophage polarization.

Immunofluorescence Staining. Briefly, macrophages on the different-coated coverslip were fixed in 4% paraformaldehyde, permeabilized with 0.25% Triton-X, and blocked by 1% BSA. Subsequently, the primary antibodies against CD68, CD163, IL-4 (Santa Cruz), and iNOS with 1:100 dilution were dropped onto coverslips and incubated overnight at 4 °C. Then the coverslips were incubated with the respective fluorescein isothiocyanate-conjugated or tetramethylrhodamine isothiocyanate-conjugated secondary antibody for 30 min, followed by 5 min of nuclear staining with DAPI. The samples were observed with a Zeiss laser-scanning microscope (LSM 510) coupled to a LSM 5 release 4.2 software.

Quantitative Real-Time Polymerase Chain Reaction. Total RNA from cell lysates was extracted with Trizol reagent (Invitrogen), and cDNA was synthesized using SuperScript III (Invitrogen) and stored at −20 °C. Real-time PCR was carried out using gene-specific primers and SYBR Green (Invitrogen) on 7900HT Fast Time PCR. The primers synthesized were as follows: Human-GAPDH, GGAGCGAGATCCCTCCAAAAT and GGCTGTTGTCATACTTCTCATGG; Human-Arg-1, CTTGGCAAAAGACTTATCCTTAG and ATGACATGGACACATAGTACCTTTC; Human-IL-10, TCAAGGCGCATGTGAACTCC and GATGTCAAACTCACTCATGGCT; and Human-IL-1β, ATGGCTTATTACAGTGGCA and GTAGTGGTGGTCGGAGATT.

Flow Cytometry. The surface markers of M1/M2 macrophages were examined by flow cytometry. The cells were isolated by trypsinization after cultured for 3 days, incubated with antibodies against CD68, CD163, and TNF-α (Abcam) at 1:50 dilution for 1 h, and then treated for 30 min with a Dylight 488-antimouse secondary antibody. The analysis of stained cells was performed on the Accuri-C6 (BD Bioscience).

Macrophage Morphology Analysis. For SEM observation, macrophages were fixed in 2% glutaraldehyde, dehydrated in a graded ethanol series (30%−100%), and examined by SEM at 15 kV. For TEM observation, macrophages seeded on different scaffolds were detached by trypsinization, followed by centrifugalization. The cells were fixed in 1% osmium tetroxide, embedded in epoxy resin, sectioned with an ultramicrotome (Leica), and collected on copper grids.

Cytokine Measurements by Enzyme-Linked Immunosorbent Assay. The supernatants of human THP-1 derived macrophages cultured on NEMC or HIMC were collected at day 7 and stored at −80 °C before use. The secretion of major M2-associated cytokines, IL-4 and IL-10, was examined with ELISA kits (R&D systems) following the manufacturer's guidance.

Human Bone Marrow Mesenchymal Stem Cells Cultured with THP-1 Supernatants. *Cell Culture.* To investigate whether macrophages in response to scaffolds could regulate osteogenesis of MSCs, human bone marrow MSCs were cultured with supernatants of THP-1 derived macrophages seeded on HIMC and NEMC, respectively. The supernatants of macrophages seeded on HIMC (HIMC + THP-1) or NEMC (NEMC + THP-1) were collected. The culture medium only placed on HIMC (HIMC) or NEMC (NEMC) was set as a control. The MSCs were isolated using a previously described method,[48] cultured in a regular medium, and supplemented with the collected supernatant at a ratio of 1:1.

Bone-Related Gene and Protein Expressions of Human Bone Marrow MSCs. After MSCs were cultured with the supernatants for 7 and 14 days, the osteogenic genes such as Runx2 and BMP2 were evaluated by real-time PCR and Western blot. For PCR, the primers synthesized were as follows: Human-Runx2, CACTGGCGCTGCAACAAGA and CATTCCGGAGCTCAGCAGAATAA; and Human-BMP2, ACTACCAGAAACGAGTGGGAA and GCATCTGTTCTCGGAAAACCT.

For Western blot, total proteins in cell lysates were harvested with a lysis solution, separated by 10% SDS-PAGE gels, and then transferred to polyvinylidene difluoride membranes and blocked in 5% nonfat milk. Subsequently, Runx2 antibody (1:1000, Abcam) was dropped onto the membranes and incubated overnight at 4 °C. The membranes were then treated with a horseradish peroxidase-conjugated secondary antibody, and protein bands were detected by enhanced chemiluminescence. Each experiment was performed three times to achieve comparable results. The relative density was measured using ImageJ 1.37v software (Wayne Rasband).

Alizarin Red S Staining. To detect mineral nodule formation, ARS staining was performed on day 21 after human bone marrow MSCs were cultured in the osteogenic medium supplemented with the collected supernatant at a ratio of 1:1. After removing the medium, MSCs were rinsed with ddH_2O, fixed in 4% paraformaldehyde, and stained with 2% ARS. The stained MSCs were observed using a Zeiss light microscopy and quantified by optical density measurement at 562 nm.

Osteogenic Differentiation of MSCs Stimulated by IL-4. *Protein Expressions.* The human bone marrow MSCs were cultured with regular medium supplemented with 20 ng/mL IL-4 for 7 and 14 days. The osteogenic protein expressions of Runx2 and BMP2 were evaluated by Western blot as stated before. To observe mineralized nodules, ARS staining was performed on day 21 after MSCs were cultured in the osteogenic medium with or without IL-4.

IL-4 Neutralization. To block the effect of IL-4, we used an IL-4 neutralizing antibody (20 ng/mL or 50 ng/mL, BD Bioscience) to reduce the content of IL-4 in the supernatants from the HIMC + THP-1 group. The human bone marrow MSCs were cultured with regular medium supplemented with pretreated supernatant for 7 days. The

DOI: 10.1021/acsnano.9b00489
ACS Nano 2019, 13, 6581−6595

protein expressions of Runx2 and BMP2 were evaluated by Western blot as stated before.

Statistical Analysis. All *in vitro* and *in vivo* data were analyzed using one-way analysis of variance (ANOVA) and Tukey's *posthoc* multiple comparion tests at $\alpha = 0.05$. For the modulus analysis, Kruskal–Wallis ANOVA multiple comparion tests were used because the normality and homoscedasticity assumptions of the data set were violated.

ASSOCIATED CONTENT

Supporting Information

The Supporting Information is available free of charge on the ACS Publications website at DOI: 10.1021/acsnano.9b00489.

Figures S1–S7 (PDF)

AUTHOR INFORMATION

Corresponding Author

*E-mail: orthoyan@bjmu.edu.cn.

ORCID

Yan Liu: 0000-0002-8193-6729

Author Contributions

Y.L. and C.W. designed the experiments. S.J., D.H., D.L., Y.W., M.Y., Y.F., B.G., Z.L., and T.Z. performed the experiments. S.J., Y.L., Y.Z., and C.W. analyzed the data and wrote the paper. All authors reviewed the paper.

Notes

The authors declare no competing financial interest.

ACKNOWLEDGMENTS

This work was supported by the Projects of Beijing Nova Programme Interdisciplinary Cooperation no. Z181100006218135 (Y.L. and D. L.), National Science Foundations of China no. 81871492 (Y.L.), no. 81571815 (Y.L.), and no. 81600893 (D.H.), and Beijing New-star Plan of Science and Technology no. Z171100001117018 (Y.L.).

REFERENCES

(1) Hollister, S. J. Porous Scaffold Design for Tissue Engineering. *Nat. Mater.* **2005**, *4*, 518–524.

(2) Taylor, D.; Hazenberg, J. G.; Lee, T. C. Living with Cracks: Damage and Repair in Human Bone. *Nat. Mater.* **2007**, *6*, 263–268.

(3) Londono, R.; Badylak, S. F. Biologic Scaffolds for Regenerative Medicine: Mechanisms of *In Vivo* Remodeling. *Ann. Biomed. Eng.* **2015**, *43*, 577–592.

(4) Sicari, B. M.; Rubin, J. P.; Dearth, C. L.; Wolf, M. T.; Ambrosio, F.; Boninger, M.; Turner, N. J.; Weber, D. J.; Simpson, T. W.; Wyse, A.; Brown, E. H.; Dziki, J. L.; Fisher, L. E.; Brown, S.; Badylak, S. F. An Acellular Biologic Scaffold Promotes Skeletal Muscle Formation in Mice and Humans with Volumetric Muscle Loss. *Sci. Transl. Med.* **2014**, *6*, 234ra58.

(5) Sadtler, K.; Estrellas, K.; Allen, B. W.; Wolf, M. T.; Fan, H.; Tam, A. J.; Patel, C. H.; Luber, B. S.; Wang, H.; Wagner, K. R.; Powell, J. D.; Housseau, F.; Pardoll, D. M.; Elisseeff, J. H. Developing a Pro-Regenerative Biomaterial Scaffold Microenvironment Requires T Helper 2 Cells. *Science* **2016**, *352*, 366–370.

(6) Zhang, W.; Zhao, F.; Huang, D.; Fu, X.; Li, X.; Chen, X. Strontium-Substituted Submicrometer Bioactive Glasses Modulate Macrophage Responses for Improved Bone Regeneration. *ACS Appl. Mater. Interfaces* **2016**, *8*, 30747–30758.

(7) Bartneck, M.; Heffels, K. H.; Pan, Y.; Bovi, M.; Zwadlo-Klarwasser, G.; Groll, J. Inducing Healing-Like Human Primary Macrophage Phenotypes by 3D Hydrogel Coated Nanofibres. *Biomaterials* **2012**, *33*, 4136–4146.

(8) Mantovani, A.; Biswas, S. K.; Galdiero, M. R.; Sica, A.; Locati, M. Macrophage Plasticity and Polarization in Tissue Repair and Remodelling. *J. Pathol.* **2013**, *229*, 176–185.

(9) Martinez, F. O.; Sica, A.; Mantovani, A.; Locati, M. Macrophage Activation and Polarization. *Front. Biosci., Landmark Ed.* **2008**, *13*, 453–461.

(10) Gordon, S. Alternative Activation of Macrophages. *Nat. Rev. Immunol.* **2003**, *3*, 23–35.

(11) Brown, B. N.; Ratner, B. D.; Goodman, S. B.; Amar, S.; Badylak, S. F. Macrophage Polarization: an Opportunity for Improved Outcomes in Biomaterials and Regenerative Medicine. *Biomaterials* **2012**, *33*, 3792–3802.

(12) Brown, B. N.; Londono, R.; Tottey, S.; Zhang, L.; Kukla, K. A.; Wolf, M. T.; Daly, K. A.; Reing, J. E.; Badylak, S. F. Macrophage Phenotype as a Predictor of Constructive Remodeling Following the Implantation of Biologically Derived Surgical Mesh Materials. *Acta Biomater.* **2012**, *8*, 978–987.

(13) Chen, Z.; Wu, C.; Gu, W.; Klein, T.; Crawford, R.; Xiao, Y. Osteogenic Differentiation of Bone Marrow MSCs by β-Tricalcium Phosphate Stimulating Macrophages *via* BMP2 Signalling Pathway. *Biomaterials* **2014**, *35*, 1507–1518.

(14) Wu, M.; Chen, G.; Li, Y. P. TGF-β and BMP Signaling in Osteoblast, Skeletal Development, and Bone Formation, Homeostasis and Disease. *Bone Res.* **2016**, *4*, 16009.

(15) Franz, S.; Rammelt, S.; Scharnweber, D.; Simon, J. C. Immune Responses to Implants - a Review of the Implications for the Design of Immunomodulatory Biomaterials. *Biomaterials* **2011**, *32*, 6692–6709.

(16) Chen, Z.; Bachhuka, A.; Han, S.; Wei, F.; Lu, S.; Visalakshan, R. M.; Vasilev, K.; Xiao, Y. Tuning Chemistry and Topography of Nanoengineered Surfaces to Manipulate Immune Response for Bone Regeneration Applications. *ACS Nano* **2017**, *11*, 4494–4506.

(17) Liu, Y.; Kim, Y. K.; Dai, L.; Li, N.; Khan, S. O.; Pashley, D. H.; Tay, F. R. Hierarchical and Non-Hierarchical Mineralisation of Collagen. *Biomaterials* **2011**, *32*, 1291–1300.

(18) Liu, Y.; Li, N.; Qi, Y. P.; Dai, L.; Bryan, T. E.; Mao, J.; Pashley, D. H.; Tay, F. R. Intrafibrillar Collagen Mineralization Produced by Biomimetic Hierarchical Nanoapatite Assembly. *Adv. Mater.* **2011**, *23*, 975–980.

(19) Liu, Y.; Luo, D.; Kou, X. X.; Wang, X. D.; Tay, F. R.; Sha, Y.; Gan, Y. H.; Zhou, Y. H. Hierarchical Intrafibrillar Nano-Carbonated Apatite Assembly Improves Nanomechanics and Cytocompatibility of Mineralized Collagen. *Adv. Funct. Mater.* **2013**, *23*, 1404–1411.

(20) Fu, Y.; Liu, S.; Cui, S. J.; Kou, X. X.; Wang, X. D.; Liu, X. M.; Sun, Y.; Wang, G. N.; Liu, Y.; Zhou, Y. H. Surface Chemistry of Nanoscale Mineralized Collagen Regulates Periodontal Ligament Stem Cell Fate. *ACS Appl. Mater. Interfaces* **2016**, *8*, 15958–15966.

(21) Liu, Y.; Liu, S.; Luo, D.; Xue, Z.; Yang, X.; Gu, L.; Zhou, Y.; Wang, T. Hierarchically-Staggered Nanostructure of Mineralized Collagen as a Bone-Grafting Scaffold. *Adv. Mater.* **2016**, *28*, 8740–8748.

(22) Zhang, C.; Yan, B. X.; Cui, Z.; Cui, S. J.; Zhang, T.; Wang, X. D.; Liu, D. W.; Yang, R. L.; Jiang, N.; Zhou, Y. H.; Liu, Y. Bone Regeneration in Minipigs by Intrafibrillarly-Mineralized Collagen Loaded with Autologous Periodontal Ligament Stem Cells. *Sci. Rep.* **2017**, *7*, 10519.

(23) Hasan, A.; Byambaa, B.; Morshed, M.; Cheikh, M. I.; Shakoor, R. A.; Mustafy, T.; Marei, H. E. Advances in Osteobiologic Materials for Bone Substitutes. *J. Tissue Eng. Regener. Med.* **2018**, *12*, 1448–1468.

(24) Kim, M.; Choe, Y. E.; Kim, G. H. Injectable Hierarchical Micro/nanofibrous Collagen-Based Scaffolds. *Chem. Eng. J.* **2019**, *365*, 220–230.

(25) Pilz, G. A.; Ulrich, C.; Ruh, M.; Abele, H.; Schäfer, R.; Kluba, T.; Bühring, H. J.; Rolauffs, B.; Aicher, W. K. Human Term Placenta-Derived Mesenchymal Stromal Cells Are Less Prone to Osteogenic Differentiation Than Bone Marrow-Derived Mesenchymal Stromal Cells. *Stem Cells Dev.* **2011**, *20*, 635–646.

(26) Loeffler, J.; Duda, G. N.; Sass, F. A.; Dienelt, A. The Metabolic Microenvironment Steers Bone Tissue Regeneration. *Trends Endocrinol. Metab.* **2018**, *29*, 99–110.

DOI: 10.1021/acsnano.9b00489
ACS Nano 2019, 13, 6581–6595

(27) Song, G.; Habibovic, P.; Bao, C.; Hu, J.; van Blitterswijk, C. A.; Yuan, H.; Chen, W.; Xu, H. H. The Homing of Bone Marrow MSCs to Non-Osseous Sites for Ectopic Bone Formation Induced by Osteoinductive Calcium Phosphate. *Biomaterials* **2013**, *34*, 2167−2176.
(28) Liu, Y.; Luo, D.; Yu, M.; Wang, Y.; Jin, S. S.; Li, Z. X.; Cui, S. J.; He, D. Q.; Zhang, T.; Wang, T.; Zhou, Y. H. Thermodynamically Controlled Self-Assembly of Hierarchically Staggered Architecture as an Osteoinductive Alternative to Bone Autografts. *Adv. Funct. Mater.* **2019**, *29*, 1806445.
(29) Sindrilaru, A.; Peters, T.; Wieschalka, S.; Baican, C.; Baican, A.; Peter, H.; Hainzl, A.; Schatz, S.; Qi, Y.; Schlecht, A.; Weiss, J. M.; Wlaschek, M.; Sunderkötter, C.; Scharffetter-Kochanek, K. An Unrestrained Proinflammatory M1Macrophage Population Induced by Iron Impairs Wound Healing in Humans and Mice. *J. Clin. Invest.* **2011**, *121*, 985−997.
(30) Wood, M. J.; Leckenby, A.; Reynolds, G.; Spiering, R.; Pratt, A. G.; Rankin, K. S.; Isaacs, J. D.; Haniffa, M. A.; Milling, S.; Hilkens, C. M. Macrophage Proliferation Distinguishes 2 Subgroups of Knee Osteoarthritis Patients. *JCI Insight* **2019**, *4*, 125325.
(31) Novak, M. L.; Koh, T. J. Phenotypic Transitions of Macrophages Orchestrate Tissue Repair. *Am. J. Pathol.* **2013**, *183*, 1352−1363.
(32) Lucas, T.; Waisman, A.; Ranjan, R.; Roes, J.; Krieg, T.; Müller, W.; Roers, A.; Eming, S. A. Differential Roles of Macrophages in Diverse Phases of Skin Repair. *J. Immunol.* **2010**, *184*, 3964−3977.
(33) Ma, J.; Liu, R.; Wang, X.; Liu, Q.; Chen, Y.; Valle, R. P.; Zuo, Y. Y.; Xia, T.; Liu, S. J. Crucial Role of Lateral Size for Graphene Oxide in Activating Macrophages and Stimulating Pro-Inflammatory Responses in Cells and Animals. *ACS Nano* **2015**, *9*, 10498−10515.
(34) Hunter, M. M.; Wang, A.; Parhar, K. S.; Johnston, M. J.; Van Rooijen, N.; Beck, P. L.; McKay, D. M. *In Vitro*-Derived Alternatively Activated Macrophages Reduce Colonic Inflammation in Mice. *Gastroenterology* **2010**, *138*, 1395−1405.
(35) Shi, X. D.; Chen, L. W.; Li, S. W.; Sun, X. D.; Cui, F. Z.; Ma, H. M. The Observed Difference of RAW264.7 Macrophage Phenotype on Mineralized Collagen and Hydroxyapatite. *Biomed Mater.* **2018**, *13*, 041001.
(36) Madsen, D. H.; Leonard, D.; Masedunskas, A.; Moyer, A.; Jürgensen, H. J.; Peters, D. E.; Amornphimoltham, P.; Selvaraj, A.; Yamada, S. S.; Brenner, D. A.; Burgdorf, S.; Engelholm, L. H.; Behrendt, N.; Holmbeck, K.; Weigert, R.; Bugge, T. H. M2-Like Macrophages are Responsible for Collagen Degradation Through a Mannose Receptor-Mediated Pathway. *J. Cell Biol.* **2013**, *202*, 951−966.
(37) Gao, C. Y.; Jin, Y.; Jia, G.; Suo, X. M.; Liu, H. F.; Liu, D. D.; Yang, X. J.; Ge, K.; Liang, X. J.; Wang, S.; Zhang, J. Y2O3 Nanoparticles Caused Bone Tissue Damage by Breaking the Intracellular Phosphate Balance in Bone Marrow Stromal Cells. *ACS Nano* **2019**, *13*, 313−323.
(38) Parkinson-Lawrence, E. J.; Shandala, T.; Prodoehl, M.; Plew, R.; Borlace, G. N.; Brooks, D. A. Lysosomal Storage Disease: Revealing Lysosomal Function and Physiology. *Physiology* **2010**, *25*, 102−115.
(39) Liu, W.; Wei, Y.; Zhang, X.; Xu, M.; Yang, X.; Deng, X. Lower Extent but Similar Rhythm of Osteogenic Behavior in hBMSCs Cultured on Nanofibrous Scaffolds *versus* Induced with Osteogenic Supplement. *ACS Nano* **2013**, *7*, 6928−6938.
(40) Chen, Z.; Mao, X.; Tan, L.; Friis, T.; Wu, C.; Crawford, R.; Xiao, Y. Osteoimmunomodulatory Properties of Magnesium Scaffolds Coated with β-Tricalcium Phosphate. *Biomaterials* **2014**, *35*, 8553−8565.
(41) Vishwakarma, A.; Bhise, N. S.; Evangelista, M. B.; Rouwkema, J.; Dokmeci, M. R.; Ghaemmaghami, A. M.; Vrana, N. E.; Khademhosseini, A. Engineering Immunomodulatory Biomaterials to Tune the Inflammatory Response. *Trends Biotechnol.* **2016**, *34*, 470−482.
(42) Loi, F.; Córdova, L. A.; Zhang, R.; Pajarinen, J.; Lin, T.; Goodman, S. B.; Yao, Z. The Effects of Immunomodulation by Macrophage Subsets on Osteogenesis *In Vitro*. *Stem Cell Res. Ther.* **2016**, *7*, 15.
(43) Bird, T. G.; Müller, M.; Boulter, L.; Vincent, D. F.; Ridgway, R. A.; Lopez-Guadamillas, E.; Lu, W. Y.; Jamieson, T.; Govaere, O.; Campbell, A. D.; Ferreira-Gonzalez, S.; Cole, A. M.; Hay, T.; Simpson, K. J.; Clark, W.; Hedley, A.; Clarke, M.; Gentaz, P.; Nixon, C.; Bryce, S. TGFβ Inhibition Restores a Regenerative Response in Acute Liver Injury by Suppressing Paracrine Senescence. *Sci. Transl. Med.* **2018**, *10*, eaan1230.
(44) Davison, N. L.; Gamblin, A. L.; Layrolle, P.; Yuan, H.; de Bruijn, J. D.; Barrère-de Groot, F. Liposomal Clodronate Inhibition of Osteoclastogenesis and Osteoinduction by Submicrostructured Beta-Tricalcium Phosphate. *Biomaterials* **2014**, *35*, 5088−5097.
(45) Domaschke, H.; Gelinsky, M.; Burmeister, B.; Fleig, R.; Hanke, T.; Reinstorf, A.; Pompe, W.; Rösen-Wolff, A. *In Vitro* Ossification and Remodeling of Mineralized Collagen I Scaffolds. *Tissue Eng.* **2006**, *12*, 949−958.
(46) Sun, J. L.; Jiao, K.; Niu, L. N.; Jiao, Y.; Song, Q.; Shen, L. J.; Tay, F. R.; Chen, J. H. Intrafibrillar Silicified Collagen Scaffold Modulates Monocyte to Promote Cell Homing, Angiogenesis and Bone Regeneration. *Biomaterials* **2017**, *113*, 203−216.
(47) Schemitsch, E. H. Size Matters: Defining Critical in Bone Defect Size. *J. Orthop. Trauma* **2017**, *31*, S20−S22.
(48) Cai, S.; Tsui, Y. P.; Tam, K. W.; Shea, G. K.; Chang, R. S.; Ao, Q.; Shum, D. K.; Chan, Y. S. Directed Differentiation of Human Bone Marrow Stromal Cells to Fate-Committed Schwann Cells. *Stem Cell Rep.* **2017**, *9*, 1097−1108.

DOI: 10.1021/acsnano.9b00489
ACS Nano 2019, 13, 6581−6595